Published in final edited form as:
Neuroimage. 2012 January 16; 59(2): 1451–1460. doi:10.1016/j.neuroimage.2011.08.001.

Direct Imaging of Macrovascular and Microvascular Contributions to BOLD fMRI in Layer IV–V of the Rat Whisker-Barrel Cortex

Xin Yu[1], **Daniel Glen**[2], **Shumin Wang**[1,*], **Stephen Dodd**[1], **Yoshiyuki Hirano**[1], **Ziad Saad**[2], **Richard Reynolds**[2], **Afonso C. Silva**[1], and **Alan P. Koretsky**[1]

[1]National Institute of Neurological Disorders and Stroke, Bethesda, MD, 20892, USA

[2]National Institute of Mental Health, National Institutes of Health, Bethesda, MD, 20892, USA

Abstract

The spatiotemporal characteristics of the hemodynamic response to increased neural activity were investigated *at the level of individual intracortical vessels* using BOLD-fMRI in a well-established rodent model of somatosensory stimulation at 11.7T. Functional maps of the rat barrel cortex were obtained at 150×150×500μm spatial resolution every 200ms. The high spatial resolution allowed separation of active voxels into those containing intracortical macro vessels, mainly vein/venules (referred to as macrovasculature), and those enriched with arteries/capillaries and small venules (referred to as microvasculature) since the macro vessel can be readily mapped due to the fast T2* decay of blood at 11.7T. The earliest BOLD response was observed within layers IV–V by 0.8s following stimulation and encompassed mainly the voxels containing the microvasculature and some confined macrovasculature voxels. By 1.2s, the BOLD signal propagated to the macrovasculature voxels where the peak BOLD signal was 2–3 times higher than that of the microvasculature voxels. The BOLD response propagated in individual venules/veins far from neuronal sources at later times. This was also observed in layers IV–V of the barrel cortex after specific stimulation of separated whisker rows. These results directly visualized that the earliest hemodynamic changes to increased neural activity occur mainly in the microvasculature and spread towards the macrovasculature. However, at peak response, the BOLD signal is dominated by penetrating venules even at layer IV–V of the cortex.

Keywords

spatial specificity; BOLD; rat; somatosensory cortex; whisker barrel

Introduction

BOLD-fMRI has become one of the most common techniques to map brain function (Bandettini et al., 1992; Kwong et al., 1992; Ogawa et al., 1992). The BOLD contrast relies on detecting the hemodynamic response to changes in neural activity. Upon functional

Address Correspondence to: Alan P. Koretsky, LFMI, NINDS, Building 10, Rm B1D728, 10 Center Drive, Bethesda, MD, 20892, koretskya@ninds.nih.gov, Tel: 301-402-9659.
[*]**Present address** Department of Electrical and Computer Engineering, Auburn University, Auburn, AL, 36894, USA

activation, the evoked neuronal/metabolic response increases the local release of vasoactive agents, causing vasodilation and local increases in cerebral blood flow (CBF)(Attwell et al., 2010; Attwell and Iadecola, 2002; Buxton, 2002; van Zijl et al., 1998). The increased inflow of oxygenated arterial blood leads to an increase in the oxy-to-deoxyhemoglobin ratio (HbO/Hb) along the local vasculature (Fox and Raichle, 1986; Malonek et al., 1997), producing a signal increase in T_2^*-weighted MR images(Ogawa et al., 1990; Thulborn et al., 1982). Thus, the spatial specificity of fMRI is limited by the spatiotemporal dynamics of the functional hemodynamic response (HRF) (Harel et al., 2006; Kim and Ugurbil, 2003; Ugurbil et al., 2003).

Previous measurements of the functional hemodynamic response to visual stimulation estimated the full-width-at-half-maximum (FWHM) of the BOLD spatial point-spread function (PSF) to be in the range of 1.7–3.9 mm in human subjects (Engel et al., 1997; Kim et al., 2004; Parkes et al., 2005; Shmuel et al., 2007; Turner, 2002; Yacoub et al., 2005) and 470μm in the cat visual cortex (Duong et al., 2001). Recently, in studying the reorganization of the primary somatosensory cortex a PSF of approximately 300–400μm FWHM was also reported(Yu et al., 2010). Thus, it is clear that the spread through the vasculature can limit the spatial specificity of BOLD fMRI. In particular, large draining veins on the surface lead to mislocalization of BOLD signals even at high magnetic field (Keilholz et al., 2006; Kim et al., 2004; Kim et al., 1994; Lai et al., 1993; Lu et al., 2004; Ugurbil et al., 2003). In contrast to BOLD fMRI, other methods, such as arterial spin labeling MRI, or cerebral blood volume MRI, have been proposed to suppress the macrovacular effect (Bolan et al., 2006; Duong et al., 2001; Lu et al., 2003; Lu et al., 2004; Williams et al., 1992; Zhao et al., 2005). However, BOLD fMRI is still the most popular functional mapping method due to the robust signal and ease of acquisition. Two major strategies have been used to eliminate the contribution of large draining veins. One strategy relies on differentiating the intra/extra-vascular dephasing properties of spins surrounding large vessels, such as spin-echo sequences or phase-dependent elimination of voxels (Duong et al., 2003; Goense and Logothetis, 2006; Menon, 2002; Ugurbil et al., 2003; Zhao et al., 2004). Another strategy relies on measuring the spatial and temporal response of the BOLD HRF. By estimating the time-dependent PSF, the initial phase of the BOLD HRF has been reported to be more spatially specific than the later phase (Goodyear and Menon, 2001; Lee et al., 1995; Shmuel et al., 2007; Silva and Koretsky, 2002). However, due to the limited spatial resolution of typical fMRI experiments, there are no studies to analyze the time-dependent contributions from microvasculature and macrovasculature to BOLD signals in the deep cortex at the level of individual vessels with BOLD fMRI.

Previously, it has been reported that there is an early onset of positive BOLD signal changes in the deep somatosensory cortex of the rat ~600ms after stimulation (Hirano et al., 2011; Silva and Koretsky, 2002). This early positive BOLD response is significantly shorter than the half-transit time of ~1.7s from arteries to veins measured by *in vivo* optical imaging (Hutchinson et al., 2006; Masamoto et al., 2010), providing evidence that fMRI changes occur before the oxy-hemoglobin can enter large veins. Based on these previous results, it may be expected that analysis of the BOLD HRF in the interval of 0.6–1.7s following stimulus onset will reduce the macrovascular contributions to the BOLD signal. In the present work, fMRI experiments at high spatial (150×150×500μm) and temporal (200ms) resolution were performed to investigate the spatiotemporal characteristics of the BOLD HRF in the time interval of 0.6–1.6s following stimulation of the whisker pad in chloralose-anesthetized rats.

Material and Methods

Animal usage

Fifteen male *Sprague*-Dawley rats were imaged at 8–9 weeks of age. The high spatiotemporal EPI images (200ms TR) were acquired from eleven rats. Among of the eleven rats, coronal EPI slices were acquired from 7 rats and horizontal EPI slices were acquired from 6 rats. The EPI images (800ms TR) were acquired from the other 4 rats.

Animal preparation for functional MRI

A detailed procedure is described in the previous study(Yu et al., 2010). To briefly describe the preparation procedure, rats were initially anesthetized with isoflurane. Each rat was orally intubated and placed on a mechanical ventilator throughout the surgery and the experiment. Plastic catheters were inserted into the right femoral artery and vein to allow monitoring of arterial blood gases and administration of drugs. After surgery, all animals were given i.v. bolus of α-chloralose (80mg/kg) and isoflurane was discontinued. Anesthesia was maintained with a constant infusion of α-chloralose (26.5mg/kg/hr). The rats were placed on a heated water pad to maintain rectal temperature at ~37°C while in the magnet. Each animal was secured in a head holder with a bite bar to prevent head motion. End-tidal CO_2, rectal temperature, tidal pressure of ventilation, heart rate, and arterial blood pressure were continuously monitored during the experiment. Arterial blood gas levels were checked periodically and corrections were made by adjusting respiratory volume or administering sodium bicarbonate to maintain normal levels when required. An i.v. injection of pancuronium bromide (4 mg/kg) was given once per hour to reduce the motion artifacts.

MRI image acquisition

All images were acquired with an 11.7 T/31 cm horizontal bore magnet (Magnex, Abingdon, UK), interfaced to an AVANCE III console (Bruker, Billerica, MA) and equipped with a 12 cm gradient set, capable of providing 100 G/cm with a rise time of 150μs(Resonance Research, MA). A custom-built 9 cm diameter quadrature transmitter coil is attached to the gradient. A 1 cm diameter surface receive coil or 4-coil cortical array with transmitting/receiving decoupling device were used during imaging acquisition. 2D gradient-echo EPI sequences were used for the fMRI studies. Setup included shimming, adjustments to echo spacing and symmetry, and B0 compensation. Using the four-array coil, a single shot sequence with a 128 × 64 matrix on a coronal slice was run with the following parameters: effective echo time (TE) 18ms, repetition time (TR) 200ms, bandwidth 278kHz, flip angle 25°, field of view (FOV) 1.92 × 0.96 cm. Anatomical MRI images in the same orientation was acquired using FLASH sequence with the following parameter: TE 5.5ms, TR 450ms, flip angle 30°, matrix 256 × 128. Using the single surface coil, a single shot sequence with a 64 × 64 matrix was run with the following parameters: effective TE 18ms, TR 800ms, bandwidth 138kHz, flip angle 45°, FOV 0.96 × 0.96 cm. The slice thickness was 500μm. To clarify the contribution of inflow effects on the BOLD signal changes on vessel voxels, a single shot sequence with 128 × 64 matrix on a horizontal slice was run with the following parameters: TE18ms, TR 1.6s, flip angle 60°, FOV 1.92 × 0.96 cm (the same sequence setup was also applied with TR at 0.2s with flip angle 25° and 0.8s with flip angle 45°). According to the rat brain atlas by Paxinos, the coronal 2D slice was positioned to bregma −2.0 to −2.5mm to cover the whisker barrel somatosensory area of the animals. The angle of the horizontal slice was set at 50° to the horizontal line and the slice center was set at 0.95mm cortical depth to cover the IV–V layer of the barrel cortex. Block design stimulation paradigm was applied in this study. For the EPI sequence with 200ms TR, the paradigm consisted of 100 dummy scans to reach steady state; followed by 80 scans during rest, 20 scans (4s) during electrical stimulation, and 80 scans during rest, which is repeated 8 times (880 scans were acquired overall). For the EPI sequence with 800ms TR, the paradigm

consisted of 20 dummy scans to reach steady state, followed by 20 scans during rest, 5 scans (4s) during electrical stimulation, and 20 scans during rest, which is repeated 8 times (220 scans were acquired overall). Both block designs have a total experiment time of 2 min 56s. For the EPI sequence with1.6s TR, the paradigm consisted of 20 dummy scans to reach steady state, followed by 10 scans during rest, 5 scans (8s) during electrical stimulation, and 10 scans during rest, which is repeated 8 times (130 scans were acquired overall). 16 –18 multiple trials were repeated for the block design with TR at 200ms and 6–8 trials were repeated for the block design with TR at 800ms and 1.6s.

Whisker pad stimulation design

Electrical stimulation of the whisker pad was described in our previous study(Yu et al., 2010). A homemade electrode pad with five pins (one cathode in the center of a 5×5 mm square with four anodes at each corner). The current delivered to the whisker pad covers a large area (5×5 mm), which could spread to activate a large barrel area. A World Precision Instruments stimulator (WPI, FL) supplied 2.5 mA, 300 μs pulses repeated at 3Hz to the whisker pad upon demand. To stimulate different rows of the whisker pad, a two-pin electrode pad was designed with 3 mm distance between two pins. Given the current spread of the 5-pin electrode, to match a similar electrical current level, the electrical pulse was set at 0.75mA when delivered by the two-pin electrode to specific whisker rows.

Imaging Processing and Statistical Analysis

fMRI data analysis was performed using Analysis of Functional NeuroImages (AFNI) software (NIH, Bethesda) (Cox, 1996). First, a 2D registration function was applied to register EPI images to a template EPI for data acquired in the same orientation setup. The baseline level of EPI images were scaled to 100 and multiple runs of block design EPI time-courses were averaged for statistical analysis. To analyze the BOLD signal changes from single vessels, no smoothing procedure was included in the image-processing steps. The HRF was estimated by the linear regression using tent basis functions. The beta value was calculated to estimate the amplitude of BOLD response at each TR. The voxel-wise beta map is presented to illustrate the spatial pattern of the BOLD response at different time points after stimulus onset. In addition, linear regression analysis was also performed by using a fixed shape response with a gamma variate function convolved with an adjusted delta function.

The voxel-wise onset delay map is acquired by fitting the HRF of each voxel as the difference of two exponential curves (supplementary figure 1),

$$y=f/(1+e^{(a+bt)}) - f/(1+e^{(c+dt)})$$

The detail of the fitting model is described in the supplementary document. The onset delay time is defined as the time to reach half the maximum in the estimated rising exponential fitting curve.

The anatomical image was registered with the rat brain atlas slices at the corresponding position from bregma −2.0 to −2.5mm. A diagram of the image/atlas registration and ROI definition is included in supplementary figure 2. The ROI of the barrel cortex in the coronal EPI images is defined based on the registered rat brain atlas with minor adjustment to cover the penetrating vessels across the barrel cortex and adjacent upper lip area. The ROI of the barrel cortex in the horizontal EPI images is defined by a 2.4×2.4mm square that covers the major portion of the barrel cortex ranging from bregma −0.5 to −3.0mm. On the averaged EPI images, a spatial uniformity correction was performed using the AFNI function

3dLocalstat to normalize the signal intensity of voxels in a 5×5 kernel. The signal intensity of the image was normalized from 0 to 1. The vessel ROI is defined based on the signal intensity of voxels in the EPI images. For the coronal EPI images, a threshold of 0.5 was used to distinguish the vessel and tissue ROIs. For the horizontal EPI images, the vessel voxels have less partial volume effects from the adjacent tissue regions since most of the intracortical vessels are perpendicular to the 500um slice. The threshold was set at 0.25 to distinguish the vessel ROI from tissue ROI. In the barrel cortex ROI, the vessel/tissue ROIs were defined specifically for each animal since the vessel distribution is different across subject. The cortical layer ROIs were uniform across animals.

Finally, a paired Student's t-test was performed to compare the mean beta value between the tissue and vessel ROIs and the error bar is the standard deviation in each graph.

Results

The spatiotemporal pattern of hemodynamic responses of the barrel cortex

High-resolution coronal EPI images (150×150×500μm) were acquired to visualize intracortical vessels penetrating the barrel cortex (Figure 1A). The dark stripes in the barrel cortex were composed of voxels with lower signal intensity due to faster T2* decay. For visualization purposes, signal intensity correction was performed to remove the heterogeneous B_1 signal profile of the surface coil (Figure 1B). This procedure allowed better visualization of the intracortical macro vessels. The spatial pattern of the BOLD HRF to bilateral stimulation of the rat whisker pad (4s on / 16s off) is shown at 200ms intervals, from stimulus onset to 16s following stimulation (Figure 1C). BOLD signal increases were first observed between 0.8–1.0s after stimulation. Around 1.2s after stimulation, active voxels appeared as bright stripes in the locations of the penetrating macro vessels. This spatial pattern persisted during the rest of the 4s stimulus period, with the BOLD signal intensity peaking 2s following stimulus onset. Once the stimulus ceased, the amplitude of the BOLD HRF decreased and by 8s after stimulation a small negative undershoot, which resolved by 10s after stimulation, was observed in the barrel cortex (Figure 1C). BOLD activation could be observed along a single macro vessel penetrating the white matter and crossing back to the cortex remote from the barrel cortex (Figure 1C). Single vessels penetrating the white matter were also observed in another two rats, showing activation 0.5 to 1.5 mm away from the stimulated barrel cortex (Figure 1D).

Spatial pattern of early onset BOLD responses

The previous experiment showed that intracortical vessels start dominating the BOLD signal as early as 1.2s after stimulus onset. To better understand how the cortical vasculature influences the spatiotemporal pattern of the BOLD HRF, single voxel analysis was performed. Two individual voxels in layer IV–V were selected to illustrate the temporal profile of BOLD response: one located in the low MRI signal intensity area corresponding to a penetrating macro vessel (macro vessel voxel), and the other in the adjacent high MRI signal intensity corresponding to the parenchyma (tissue voxel) which is enriched with microvasculature (Figure 2A). The macro vessel voxel had higher peak BOLD signal changes than the tissue voxel by a factor of 2.5 (Figure 2B, raw data; 2C, HRF), demonstrating a substantial macrovascular contribution to the BOLD signal at high magnetic fields even in the intracortical region. However, the BOLD HRF started earlier in the tissue voxel than in the macro vessel voxel (Figure 2C), suggesting the BOLD response starts in the parenchyma before progressing to macro vessels.

Figure 3 shows the time-dependent spatial pattern of the BOLD HRF from 0.8s to 1.4s in multiple rats. It is clear that by 0.8s after stimulation a large number of active voxels were

located on the tissue voxels between macro vessels (Figure 2B). The spatial distribution of active voxels did not match the location of macro vessels at 0.8s after stimulation. Activation propagated to the macro vessel voxels by 1.0s, which then dominated the BOLD contrast after 1.2s. To compare the early temporal difference of BOLD response between voxels, an onset delay map was estimated by dual-exponential fitting of the rising and falling phase of BOLD HRF in each voxel (detailed description in the supplementary notes). The onset delay map showed a clear trend of longer onset time in the macro vessel voxels than in the tissue voxels (Figure 3C, Supplementary Figure 1). To quantify BOLD signal changes between the macro vessel voxels and the surrounding tissue voxels, the HRF in two ROIs containing the tissue and the macro vessel voxels were analyzed (Figure 3D, inset figure is a representative tissue and macro vessel ROIs from one rat). The tissue and macro vessel ROIs were defined based on the signal intensity of the voxels in EPI images. A detailed criterion is described in the Method section. Paired two-sample Student's t-test showed that the BOLD signal of the tissue ROI at 0.8s after stimulation is significantly higher than that of the macro vessel ROI, by 65±12% (Figure 3E, inset). This compares to the peak BOLD response at 3.0s, showing the BOLD signal in the macro vessel ROI was ~1.67 times higher (Figure 3D). Although the higher BOLD signal of tissue ROIs at 0.8s is small in comparison to the higher peak response of macro vessel ROIs (Figure 3D), it indicates distinct micro/macro-vascular contributions to the BOLD signal at the early time after stimulation.

Layer specific spatial pattern of early onset BOLD responses

In the previous analysis, the tissue and macro vessel ROIs span along all layers of the cortex, possibly diminishing the difference in onset delays previously found across the cortical layers (Silva and Koretsky, 2002). The BOLD response was analyzed in layer-specific ROI regions (Figure 4A). The barrel cortex was separated into three sections (Layer I–III, IV–V, and VI) based on the cortical depth measured from the high spatial resolution EPI images (Figure 4A, inset). The time-courses from the laminar ROIs show that the BOLD HRF in layers IV–V rises faster following stimulus onset than the responses in layers I–III and layer VI (Figure 4B, C). The order of onset times in the different cortical layers is consistent with a previous report (Silva and Koretsky, 2002).

Due to potential partial volume effects through the 500μm slice thickness and the difference in onset times through the depth of the cortex, data were acquired in the horizontal orientation with a 50° angle to the horizontal line (Figure 5A). The slice covered the barrel cortex from 0.7 to 1.2 mm deep from the surface, i.e. the central location of Layer IV–V barrel cortex. In this orientation, it is likely that voxels containing the large vessels penetrating the slice had less partial volume effects since they now span the entire slice. Figure 5 shows the BOLD HRF measured from a 500μm-thick slice containing layers IV–V, prescribed as indicated in Figure 5A to be centered in the whisker barrel functional region as shown in Figure 4A. This slice orientation is perpendicular to the penetrating vessels (Figure 5A), and so they appeared as dark dots rather than dark stripes (Figure 5B). The BOLD HRF from two individual voxels, one located in the low signal intensity area corresponding to a penetrating macro vessel, and the other in the immediately adjacent high signal intensity area corresponding to the parenchyma (tissue) area, showed an earlier onset for the tissue voxel (Figure 5C, inset). Figure 5D shows the spatial pattern of the BOLD response at 200ms intervals from 0s to 1.6s following stimulation. The location of macro vessels was marked by red squares based on the low signal intensity of macro vessel voxels. BOLD signal increases were first observed 0.8s after stimulation in the region surrounding the macro vessel voxels. Around 1.2s after stimulation, the macro vessel voxels became active (Figure 5D). In fact, most macro vessel voxels were not activated 0.8s after stimulus onset, but showed strong BOLD signal at 1.4s following stimulation (Figure 6A). For visualization

purposes, vessel voxels were manually highlighted with blue dotted circles (Figure 6B), or were colored green by setting a threshold based on the signal-to-noise ratio (SNR) in the EPI images (Figure 6C, details in the Method section). Group analysis showed that the BOLD signal in the tissue ROI at 0.8s was significantly higher than the macro vessel ROI by 40±10%. At 3s, the peak BOLD signal in the macro vessel ROI was ~2.08 times higher than in the tissue ROI (Figure 6D). In summary, these results demonstrated a delayed BOLD response in most of the large intracortical penetrating vessels, indicating that mapping BOLD response during the early onset time might provide better specificity to the microvasculature by excluding macro vessels.

Mapping whisker row specific BOLD responses in the barrel cortex

The time-dependent microvascular and macrovascular contributions to whisker row-specific functional maps were analyzed. To ensure that the early BOLD signal detected at 0.8s is independent of the short TR which may potentially involve inflow effects(Kim et al., 1994), the BOLD response was acquired with TR at 0.8s in block design (4s on /16s off, 8 epochs). The somatotopic representation of whisker row-B and row-D was specified at the caudal barrel area for row-B and the rostral barrel area for row-D (Figure 7A, inset) (Chapin and Lin, 1984). First, functional maps of row-B and row-D derived from a linear regression fit to the total period of the hemodynamic response are shown in Figure 7B. The two functional maps represented the expected somatotopic organization for row-B and row-D whisker barrel areas but with large overlap. Macro vessels could be identified between the two representational areas (e.g. Figure 7B, red rectangle). Time-courses of ROIs placed on one of the overlapped macro vessels showed later onset time of BOLD response in comparison to the ROIs located on the centriod of active row-B or row-D barrel area (Figure 7B, blue rectangle). Fig 7C shows the time-dependent functional maps from 0 to 3.2s after stimulation. There was a more confined activated area for the two whisker rows at 0.8s, which became overlapped on macro vessels at the late time points (Figure 7C). This result demonstrates that macrovascular contributions affect BOLD fMRI maps even at layer IV–V and that the later onset time may be used to remove the macrovascular contribution.

Discussion

The present study describes the spatiotemporal dynamics of the neurovascular coupling in the deep cortical layers of the rat barrel cortex. High spatial resolution EPI images could visualize intracortical macrovasculature and allowed separation of voxels containing large intracortical vessels from surrounding voxels enriched with microvasculature. An early positive BOLD response was observed 0.8 s following stimulus onset mainly in tissue voxels. Around 1.2s after stimulation, voxels containing intracortical macro vessels dominated the BOLD signal. Whisker row-specific barrel areas showed a more confined BOLD response at 0.8s, but were overlapped by macro vessels that drained the two active regions at later times. These results indicate that, in addition to the surface draining veins increasing the BOLD hemodynamic PSF, penetrating macro vessels contribute to the BOLD signal changes even in the deep cortical layers. By mapping the early BOLD response before the propagation of the BOLD signal to macro vessels, the microvascular contribution to the BOLD signal could be analyzed at the deep cortical layers. There is only a small signal increase at 0.8s and so sensitive detection and averaging are required at the high resolution used.

The early positive BOLD signal was detected at 0.8s after stimulus onset and initiated in layers IV–V of the cortex. This layer-specific early BOLD response is in agreement with previous BOLD-fMRI studies (Hirano et al., 2011; Jin and Kim, 2008; Siero et al., in press; Silva and Koretsky, 2002; Tian et al., 2010). Early optical and laser Doppler flowmetry studies claimed that the onset of vessel dilation and cerebral blood flow appeared first at the

superficial cortical layers or equally along the cortical depth (Hillman et al., 2007; Norup Nielsen and Lauritzen, 2001). However, a more recent two-photon microscopy study(Tian et al., 2010) indicates faster arteriole dilation onset in the deeper cortical layer consistent with the original fMRI study(Silva and Koretsky, 2002). The estimated onset time of arteriole dilation at the deeper layers was in the range of 0.25–0.7s (Tian et al., 2010). Given the early arteriole dilation onset and the reported ~1.7s transit time estimated from artery to veins (Hutchinson et al., 2006; Masamoto et al., 2010), the BOLD response detected at 0.8s can be attributed mainly to a combination of the arterioles, capillary and possibly small venules. The 0.8s onset time reported here is slightly longer than the 0.6s onset reported in a previous BOLD-fMRI study on rats (Hirano et al., 2011; Silva and Koretsky, 2002). These previous studies used a larger voxel size and so the onset difference may be caused by the lower signal-to-noise ratio due to the much smaller voxel size (150×150×500μm) used in the present study. Also noteworthy is that the 0.8s onset is much faster than what has been reported in human fMRI studies (de Zwart et al., 2005; Goodyear and Menon, 2001; Krings et al., 1999; Saad et al., 2001; Siero et al., in press). This may be because the present study has a much higher spatial and temporal resolution than is typically used in human fMRI studies. A different temporal hemodynamic response between human and rodents may also contribute to the difference (de Zwart et al., 2005; Hirano et al., 2011; Silva et al., 2007).

The hemodynamic response in deep cortical layers at the level of individual intracortical penetrating vessels was directly measured in the present study. The intracortical vasculature can be visualized by susceptibility-weighted MRI techniques (Bolan et al., 2006; Ogawa et al., 1990; Reichenbach et al., 1997). In the normal physiological state, arterial blood has a magnetic susceptibility comparable to the surrounding cortical tissue (Bolan et al., 2006; Lee et al., 1999), making identification of arteries in T_2^*-weighted images difficult. On the other hand, the elevated concentration of deoxyhemoglobin in veins induce local field distortions that lead to faster signal dephasing in the blood and adjacent cortical tissue, allowing these vessels to be identified by the dark structures visible in T_2^*-weighted EPI images. Thus, the microvasculature indentified in the present study mainly indicates the vein and venules penetrating the cortex. Previous studies indicate that these veins or venules are on average 75μm wide with an average separation ranging from 300 to 500μm (Bolan et al., 2006; Cox et al., 1993; Hutchinson et al., 2006; Stefanovic et al., 2008). The voxel size (150×150×500μm) used in the present study was small enough to allow visualization of principal cortical venules as dark stripes in the coronal images or dark dots in the horizontal images. Thus, by setting a signal intensity threshold in the T_2^*-weighted anatomical EPI images, low signal intensity voxels (macro vessel) containing intracortical macro vessels could be separated from the tissue voxels with higher signal intensity and certainly enriched with capillary vessels and small venules. However, it is likely that some small penetrating vessels were missed. Direct comparison of MRI identified vessels with histology was not included in the present study, but could be performed in future studies to better define the vasculature detected.

Separation of tissue voxels from the macro vessel voxels made it possible to directly analyze the BOLD effects from macrovasculature. It has been reported that high field functional mapping could highlight the microvascular contributions and reduce the effects of macrovasculature due to the suppression of intravascular BOLD signals by the dramatically shortened T_2^* of blood (Lee et al., 1999; Shmuel et al., 2007; Uludag et al., 2009). However, the peak BOLD response at 11.7T shown here was primarily located on the macro vessel voxels, showing two times higher signal than that of adjacent tissue voxels even in deep cortex (Figure 2, 5). Due to the limits of the spatial resolution, the signal in vessel voxels(150×150×500μm) is contributed by water protons from both vessel and surrounding tissue. The size of intracortical macro vessels ranges from ~50 to ~100μm(Bolan et al., 2006; Cox et al., 1993; Hutchinson et al., 2006; Stefanovic et al., 2008). Therefore, in most

macro vessel voxels, the water contribution from vessels is small, ranging from ~10% to ~50%. In addition, short T2* of blood at 11.7T magnetic field strength decreases the intravascular contribution further (Keilholz et al., 2006; Seehafer et al., 2010). Thus, the extravascular effects from macrovasculature are likely to dominate the BOLD signal detected by the gradient echo EPI sequence. Considering that extravascular effects should extend at least a few vessel radii, it is likely that the macrovascular voxels are dominated by extravascular effects and at peak response there is probably an extravascular effect from macro vessels in the voxels adjacent to “tissue” voxels. It may be possible to further improve the resolution to be able to directly measure the intravascular effects by mapping BOLD responses from single voxels that were small compared to vessel sizes. It has been proposed that spin-echo acquisition can decrease extravascular contributions (Duong et al., 2003; Ugurbil et al., 2003; Yacoub et al., 2003; Yacoub et al., 2007). It will be interesting to compare Gradient-Echo vs. Spin-Echo effects from individual deep cortical macro vessels in future studies.

Another cause of the high BOLD signal detected in macro vessel voxels could be due to inflow effects associated with the thin slice (500μm) and fast TR (200ms) of our EPI sequence (Kim et al., 1994). In the present study, the flip angle was adjusted accordingly to reduce inflow effects (Kim et al., 1994; Shmuel et al., 2007). In addition, when we kept the same slice thickness but increased the TR to 0.8s and 1.6s (supplementary Figure 2), the peak BOLD signal was still localized in the macro vessel voxels indicating oxy-hemoglobin effects dominated. Furthermore, results were similar from the two different slice orientations (venule in plane vs. venule through plane) where inflow effects should be different.

Previous studies used the spatial PSF to estimate the spatial specificity of BOLD responses (Engel et al., 1997; Parkes et al., 2005; Shmuel et al., 2007; Turner, 2002). By comparing the time-dependent FWHM of PSF, the initial phase of the BOLD response has been suggested to be more spatially specific than later phases (Goodyear and Menon, 2001; Shmuel et al., 2007). Our study directly demonstrated the spatial evolution of BOLD response in the cerebral vasculature at the level of single venules and supports the idea that better spatial specificity can be obtained at the initial phase of the BOLD response. At 0.8s after stimulation, the increased BOLD signal did not appear in most of the macro vessel voxels, but was present in adjacent tissue voxels (Figure 6). The BOLD signal at 0.8s in the tissue voxels is only 25–35% of its peak value; however, this was 45–65% higher than that in the macro vessel ROI at this time indicating a large weighting to the microvasculature. This relative contrast between micro and macro vasculature switches at about 1.2s and by peak response the BOLD signal is two times higher in macro vessel ROIs. Extracellular effects from the macro vessels probably extend to the tissue voxels during peak response so that the two fold difference probably underestimates the dominating effect of the macro vessels. The consequences of this could be seen in the spatial pattern of the whisker row-specific BOLD responses. A more confined region at 0.8s was mapped after stimulation than at the later time points. Individual activated macro vessels at the later time after stimulation spread over a large spatial scale, leading to mislocation of the BOLD signal on a millimeter scale. Indeed, the late-onset individual vessels running into white matter and back through grey matter were 1–1.5 mm away from the activated barrel cortex (Figure 1). In the row-specific BOLD functional maps, a remote penetrating venule that drained the two active barrel areas showed a BOLD response at 1.6s after stimulation (Figure 7). In addition, we also observed small, steady-state negative BOLD signal changes in the cortical area adjacent to the activated barrel cortex in the row-specific stimulation paradigm (supplementary figure 3). This result opens the possibility of addressing the contribution of macro vessels to the negative BOLD response in future studies.

Conclusion

In this study, the evoked BOLD response can be detected as early as 0.8s after the stimulus onset in the rodent barrel cortex. In contrast, the later onset of BOLD responses in individual macro vessels as compared to tissue voxels has been demonstrated. In addition, the peak BOLD signal of macro vessel voxels is at least twice as large as that of the tissue vboxels. Thus, in addition to draining veins on the cortical surface, intracortical macro vessels can lead to mislocation of BOLD fMRI. Since the macro vessels are located 300–500μm apart, this limits the spatial specificity of peak BOLD fMRI mapping even in layers IV–V of cortex. In summary, the distinct spatiotemporal contribution of microvasculature and macrovasculature can be imaged from deep cortex and has the potential to improve the spatial specificity of fMRI mapping. Furthermore, the ability to detect changes in individual macro vessels from deep cortex will enable directly investigating the specificity of spin-echo BOLD-fMRI, CBV and arterial spin labeling approaches to brain mapping.

Supplementary Material

Refer to Web version on PubMed Central for supplementary material.

Abbreviations

fMRI	functional magnetic resonance imaging
BOLD	blood oxygen level dependent
SI	primary somatosensory cortex
EPI	echo planar imaging
Hb	deoxyhemoglobin
HbO	oxygenated hemoglobin
SNR	signal-noise ration
CNR	contrast-noise ratio

Acknowledgments

This research was supported by the Intramural Research Program of the NIH, NINDS. We thank Ms. Nadia Bouraoud and Ms. Kathryn Sharer for their technical support.

References

Attwell D, Buchan AM, Charpak S, Lauritzen M, Macvicar BA, Newman EA. Glial and neuronal control of brain blood flow. Nature. 2010; 468:232–243. [PubMed: 21068832]

Attwell D, Iadecola C. The neural basis of functional brain imaging signals. Trends Neurosci. 2002; 25:621–625. [PubMed: 12446129]

Bandettini PA, Wong EC, Hinks RS, Tikofsky RS, Hyde JS. Time course EPI of human brain function during task activation. Magn Reson Med. 1992; 25:390–397. [PubMed: 1614324]

Bolan PJ, Yacoub E, Garwood M, Ugurbil K, Harel N. In vivo micro-MRI of intracortical neurovasculature. Neuroimage. 2006; 32:62–69. [PubMed: 16675271]

Buxton, RB. Introduction to Functional Magnetic Resonance Imaging: Principles and Techniques. Cambridge: Cambridge University Press; 2002.

Chapin JK, Lin CS. Mapping the body representation in the SI cortex of anesthetized and awake rats. J Comp Neurol. 1984; 229:199–213. [PubMed: 6438190]

Cox RW. AFNI: software for analysis and visualization of functional magnetic resonance neuroimages. Comput Biomed Res. 1996; 29:162–173. [PubMed: 8812068]

Cox SB, Woolsey TA, Rovainen CM. Localized dynamic changes in cortical blood flow with whisker stimulation corresponds to matched vascular and neuronal architecture of rat barrels. J Cereb Blood Flow Metab. 1993; 13:899–913. [PubMed: 8408316]

de Zwart JA, Silva AC, van Gelderen P, Kellman P, Fukunaga M, Chu R, Koretsky AP, Frank JA, Duyn JH. Temporal dynamics of the BOLD fMRI impulse response. Neuroimage. 2005; 24:667–677. [PubMed: 15652302]

Duong TQ, Kim DS, Ugurbil K, Kim SG. Localized cerebral blood flow response at submillimeter columnar resolution. Proc Natl Acad Sci U S A. 2001; 98:10904–10909. [PubMed: 11526212]

Duong TQ, Yacoub E, Adriany G, Hu X, Ugurbil K, Kim SG. Microvascular BOLD contribution at 4 and 7 T in the human brain: gradient-echo and spin-echo fMRI with suppression of blood effects. Magn Reson Med. 2003; 49:1019–1027. [PubMed: 12768579]

Engel SA, Glover GH, Wandell BA. Retinotopic organization in human visual cortex and the spatial precision of functional MRI. Cereb Cortex. 1997; 7:181–192. [PubMed: 9087826]

Fox PT, Raichle ME. Focal physiological uncoupling of cerebral blood flow and oxidative metabolism during somatosensory stimulation in human subjects. Proc Natl Acad Sci U S A. 1986; 83:1140–1144. [PubMed: 3485282]

Goense JB, Logothetis NK. Laminar specificity in monkey V1 using high-resolution SE-fMRI. Magn Reson Imaging. 2006; 24:381–392. [PubMed: 16677944]

Goodyear BG, Menon RS. Brief visual stimulation allows mapping of ocular dominance in visual cortex using fMRI. Hum Brain Mapp. 2001; 14:210–217. [PubMed: 11668652]

Harel N, Ugurbil K, Uludag K, Yacoub E. Frontiers of brain mapping using MRI. J Magn Reson Imaging. 2006; 23:945–957. [PubMed: 16649202]

Hillman EM, Devor A, Bouchard MB, Dunn AK, Krauss GW, Skoch J, Bacskai BJ, Dale AM, Boas DA. Depth-resolved optical imaging and microscopy of vascular compartment dynamics during somatosensory stimulation. Neuroimage. 2007; 35:89–104. [PubMed: 17222567]

Hirano Y, Stefanovic B, Silva AC. Spatiotemporal evolution of the functional magnetic resonance imaging response to ultrashort stimuli. J Neurosci. 2011; 31:1440–1447. [PubMed: 21273428]

Hutchinson EB, Stefanovic B, Koretsky AP, Silva AC. Spatial flow-volume dissociation of the cerebral microcirculatory response to mild hypercapnia. Neuroimage. 2006; 32:520–530. [PubMed: 16713717]

Jin T, Kim SG. Cortical layer-dependent dynamic blood oxygenation, cerebral blood flow and cerebral blood volume responses during visual stimulation. Neuroimage. 2008; 43:1–9. [PubMed: 18655837]

Keilholz SD, Silva AC, Raman M, Merkle H, Koretsky AP. BOLD and CBV-weighted functional magnetic resonance imaging of the rat somatosensory system. Magn Reson Med. 2006; 55:316–324. [PubMed: 16372281]

Kim DS, Ronen I, Olman C, Kim SG, Ugurbil K, Toth LJ. Spatial relationship between neuronal activity and BOLD functional MRI. Neuroimage. 2004; 21:876–885. [PubMed: 15006654]

Kim SG, Hendrich K, Hu X, Merkle H, Ugurbil K. Potential pitfalls of functional MRI using conventional gradient-recalled echo techniques. NMR Biomed. 1994; 7:69–74. [PubMed: 8068528]

Kim SG, Ugurbil K. High-resolution functional magnetic resonance imaging of the animal brain. Methods. 2003; 30:28–41. [PubMed: 12695101]

Krings T, Erberich SG, Roessler F, Reul J, Thron A. MR blood oxygenation level-dependent signal differences in parenchymal and large draining vessels: implications for functional MR imaging. AJNR Am J Neuroradiol. 1999; 20:1907–1914. [PubMed: 10588117]

Kwong KK, Belliveau JW, Chesler DA, Goldberg IE, Weisskoff RM, Poncelet BP, Kennedy DN, Hoppel BE, Cohen MS, Turner R, et al. Dynamic magnetic resonance imaging of human brain activity during primary sensory stimulation. Proc Natl Acad Sci U S A. 1992; 89:5675–5679. [PubMed: 1608978]

Lai S, Hopkins AL, Haacke EM, Li D, Wasserman BA, Buckley P, Friedman L, Meltzer H, Hedera P, Friedland R. Identification of vascular structures as a major source of signal contrast in high resolution 2D and 3D functional activation imaging of the motor cortex at 1.5T: preliminary results. Magn Reson Med. 1993; 30:387–392. [PubMed: 8412613]

Lee AT, Glover GH, Meyer CH. Discrimination of large venous vessels in time-course spiral blood-oxygen-level-dependent magnetic-resonance functional neuroimaging. Magn Reson Med. 1995; 33:745–754. [PubMed: 7651109]

Lee SP, Silva AC, Ugurbil K, Kim SG. Diffusion-weighted spin-echo fMRI at 9.4 T: microvascular/tissue contribution to BOLD signal changes. Magn Reson Med. 1999; 42:919–928. [PubMed: 10542351]

Lu H, Golay X, Pekar JJ, Van Zijl PC. Functional magnetic resonance imaging based on changes in vascular space occupancy. Magn Reson Med. 2003; 50:263–274. [PubMed: 12876702]

Lu H, Patel S, Luo F, Li SJ, Hillard CJ, Ward BD, Hyde JS. Spatial correlations of laminar BOLD and CBV responses to rat whisker stimulation with neuronal activity localized by Fos expression. Magn Reson Med. 2004; 52:1060–1068. [PubMed: 15508149]

Malonek D, Dirnagl U, Lindauer U, Yamada K, Kanno I, Grinvald A. Vascular imprints of neuronal activity: relationships between the dynamics of cortical blood flow, oxygenation, and volume changes following sensory stimulation. Proc Natl Acad Sci U S A. 1997; 94:14826–14831. [PubMed: 9405698]

Masamoto K, Obata T, Kanno I. Intracortical microcirculatory change induced by anesthesia in rat somatosensory cortex. Adv Exp Med Biol. 2010; 662:57–61. [PubMed: 20204771]

Menon RS. Postacquisition suppression of large-vessel BOLD signals in high-resolution fMRI. Magn Reson Med. 2002; 47:1–9. [PubMed: 11754436]

Norup Nielsen A, Lauritzen M. Coupling and uncoupling of activity-dependent increases of neuronal activity and blood flow in rat somatosensory cortex. J Physiol. 2001; 533:773–785. [PubMed: 11410634]

Ogawa S, Lee TM, Kay AR, Tank DW. Brain magnetic resonance imaging with contrast dependent on blood oxygenation. Proc Natl Acad Sci U S A. 1990; 87:9868–9872. [PubMed: 2124706]

Ogawa S, Tank DW, Menon R, Ellermann JM, Kim SG, Merkle H, Ugurbil K. Intrinsic signal changes accompanying sensory stimulation: functional brain mapping with magnetic resonance imaging. Proc Natl Acad Sci U S A. 1992; 89:5951–5955. [PubMed: 1631079]

Parkes LM, Schwarzbach JV, Bouts AA, Deckers RH, Pullens P, Kerskens CM, Norris DG. Quantifying the spatial resolution of the gradient echo and spin echo BOLD response at 3 Tesla. Magn Reson Med. 2005; 54:1465–1472. [PubMed: 16276507]

Reichenbach JR, Venkatesan R, Schillinger DJ, Kido DK, Haacke EM. Small vessels in the human brain: MR venography with deoxyhemoglobin as an intrinsic contrast agent. Radiology. 1997; 204:272–277. [PubMed: 9205259]

Saad ZS, Ropella KM, Cox RW, DeYoe EA. Analysis and use of FMRI response delays. Hum Brain Mapp. 2001; 13:74–93. [PubMed: 11346887]

Seehafer JU, Kalthoff D, Farr TD, Wiedermann D, Hoehn M. No increase of the blood oxygenation level-dependent functional magnetic resonance imaging signal with higher field strength: implications for brain activation studies. J Neurosci. 2010; 30:5234–5241. [PubMed: 20392946]

Shmuel A, Yacoub E, Chaimow D, Logothetis NK, Ugurbil K. Spatio-temporal point-spread function of fMRI signal in human gray matter at 7 Tesla. Neuroimage. 2007; 35:539–552. [PubMed: 17306989]

Siero M, Petridou N, Luijten PR, Ramsey NF. Cortical depth-dependent temporal dynamics of the BOLD response in the human brain. J Cereb Blood Flow Metab. in press.

Silva AC, Koretsky AP. Laminar specificity of functional MRI onset times during somatosensory stimulation in rat. Proc Natl Acad Sci U S A. 2002; 99:15182–15187. [PubMed: 12407177]

Silva AC, Koretsky AP, Duyn JH. Functional MRI impulse response for BOLD and CBV contrast in rat somatosensory cortex. Magn Reson Med. 2007; 57:1110–1118. [PubMed: 17534912]

Stefanovic B, Hutchinson E, Yakovleva V, Schram V, Russell JT, Belluscio L, Koretsky AP, Silva AC. Functional reactivity of cerebral capillaries. J Cereb Blood Flow Metab. 2008; 28:961–972. [PubMed: 18059431]

Thulborn KR, Waterton JC, Matthews PM, Radda GK. Oxygenation dependence of the transverse relaxation time of water protons in whole blood at high field. Biochim Biophys Acta. 1982; 714:265–270. [PubMed: 6275909]

Tian P, Teng IC, May LD, Kurz R, Lu K, Scadeng M, Hillman EM, De Crespigny AJ, D'Arceuil HE, Mandeville JB, Marota JJ, Rosen BR, Liu TT, Boas DA, Buxton RB, Dale AM, Devor A. Cortical depth-specific microvascular dilation underlies laminar differences in blood oxygenation level-dependent functional MRI signal. Proc Natl Acad Sci U S A. 2010; 107:15246–15251. [PubMed: 20696904]

Turner R. How much cortex can a vein drain? Downstream dilution of activation-related cerebral blood oxygenation changes. Neuroimage. 2002; 16:1062–1067. [PubMed: 12202093]

Ugurbil K, Toth L, Kim DS. How accurate is magnetic resonance imaging of brain function? Trends Neurosci. 2003; 26:108–114. [PubMed: 12536134]

Uludag K, Muller-Bierl B, Ugurbil K. An integrative model for neuronal activity-induced signal changes for gradient and spin echo functional imaging. Neuroimage. 2009; 48:150–165. [PubMed: 19481163]

van Zijl PC, Eleff SM, Ulatowski JA, Oja JM, Ulug AM, Traystman RJ, Kauppinen RA. Quantitative assessment of blood flow, blood volume and blood oxygenation effects in functional magnetic resonance imaging. Nat Med. 1998; 4:159–167. [PubMed: 9461188]

Williams DS, Detre JA, Leigh JS, Koretsky AP. Magnetic resonance imaging of perfusion using spin inversion of arterial water. Proc Natl Acad Sci U S A. 1992; 89:212–216. [PubMed: 1729691]

Yacoub E, Duong TQ, Van De Moortele PF, Lindquist M, Adriany G, Kim SG, Ugurbil K, Hu X. Spin-echo fMRI in humans using high spatial resolutions and high magnetic fields. Magn Reson Med. 2003; 49:655–664. [PubMed: 12652536]

Yacoub E, Shmuel A, Logothetis N, Ugurbil K. Robust detection of ocular dominance columns in humans using Hahn Spin Echo BOLD functional MRI at 7 Tesla. Neuroimage. 2007; 37:1161–1177. [PubMed: 17702606]

Yacoub E, Van De Moortele PF, Shmuel A, Ugurbil K. Signal and noise characteristics of Hahn SE and GE BOLD fMRI at 7 T in humans. Neuroimage. 2005; 24:738–750. [PubMed: 15652309]

Yu X, Wang S, Chen DY, Dodd S, Goloshevsky A, Koretsky AP. 3D mapping of somatotopic reorganization with small animal functional MRI. Neuroimage. 2010; 49:1667–1676. [PubMed: 19770051]

Zhao F, Wang P, Hendrich K, Kim SG. Spatial specificity of cerebral blood volume-weighted fMRI responses at columnar resolution. Neuroimage. 2005; 27:416–424. [PubMed: 15923128]

Zhao F, Wang P, Kim SG. Cortical depth-dependent gradient-echo and spin-echo BOLD fMRI at 9.4T. Magn Reson Med. 2004; 51:518–524. [PubMed: 15004793]

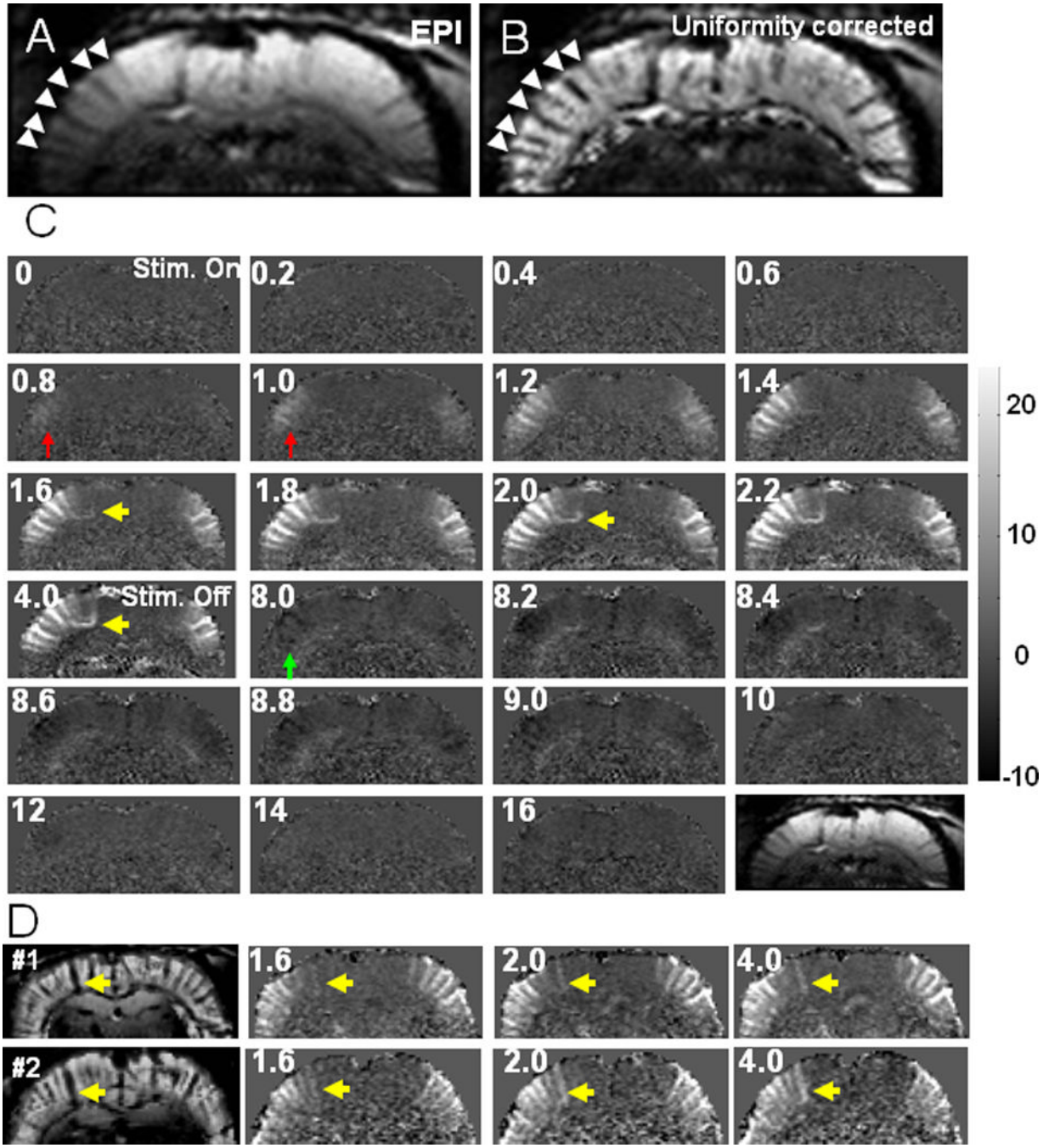

Figure 1.

The spatial pattern of hemodynamic response in the coronal EPI slice. A coronal EPI slice covering the barrel cortex was acquired in rats with bilateral whisker pad stimulation. The intracortical macro vessels (white arrowhead) are visualized in the averaged 2D EPI image (A) and the uniformity corrected image (B). The spatial pattern of BOLD response at every 200ms is represented in gray-scale beta maps(C). BOLD responses first appeared at 0.8–1.0s after stimulation (red arrow) and peaked at macro vessels (bright stripes) in the later time. The undershoot of BOLD responses appeared at 8s after stimulation (green arrow). BOLD responses in a single macro vessel penetrating the white matter appeared at 1.6s after

stimulation (yellow arrow). BOLD responses in macro vessels penetrating the white matter were observed in another two rats (D, yellow arrow).

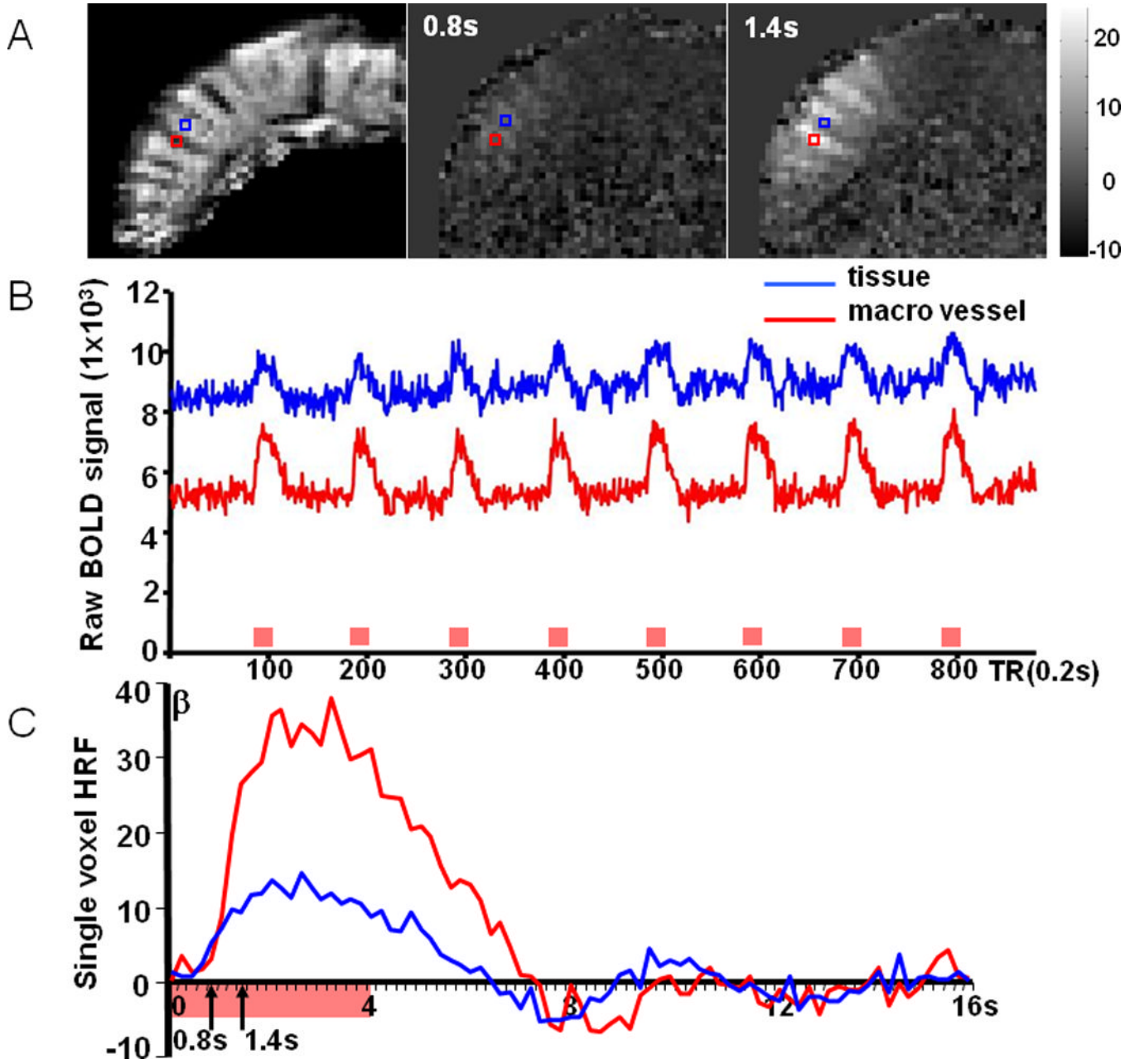

Figure 2.

The hemodynamic response of representative single voxels. One voxel is located in the center of a macro vessel (red) and the other in the tissue (blue) surrounding the macro vessel at Layer IV–V of the barrel cortex (A, EPI). Gray-scale beta maps at 0.8s and 1.4s are shown to highlight the early BOLD signal response of the two voxels (A). The time-course of BOLD response (4s on / 16s off, 8 epochs) and the HRF of the two voxels are shown in B and C. The baseline signal intensity of vessel voxel is much lower than that of the tissue voxel (B). In the HRF, the BOLD signal of the tissue voxel (blue) is higher than that of the vessel voxel at 0.8s after stimulation, which becomes opposite at 1.4s after stimulation (C).

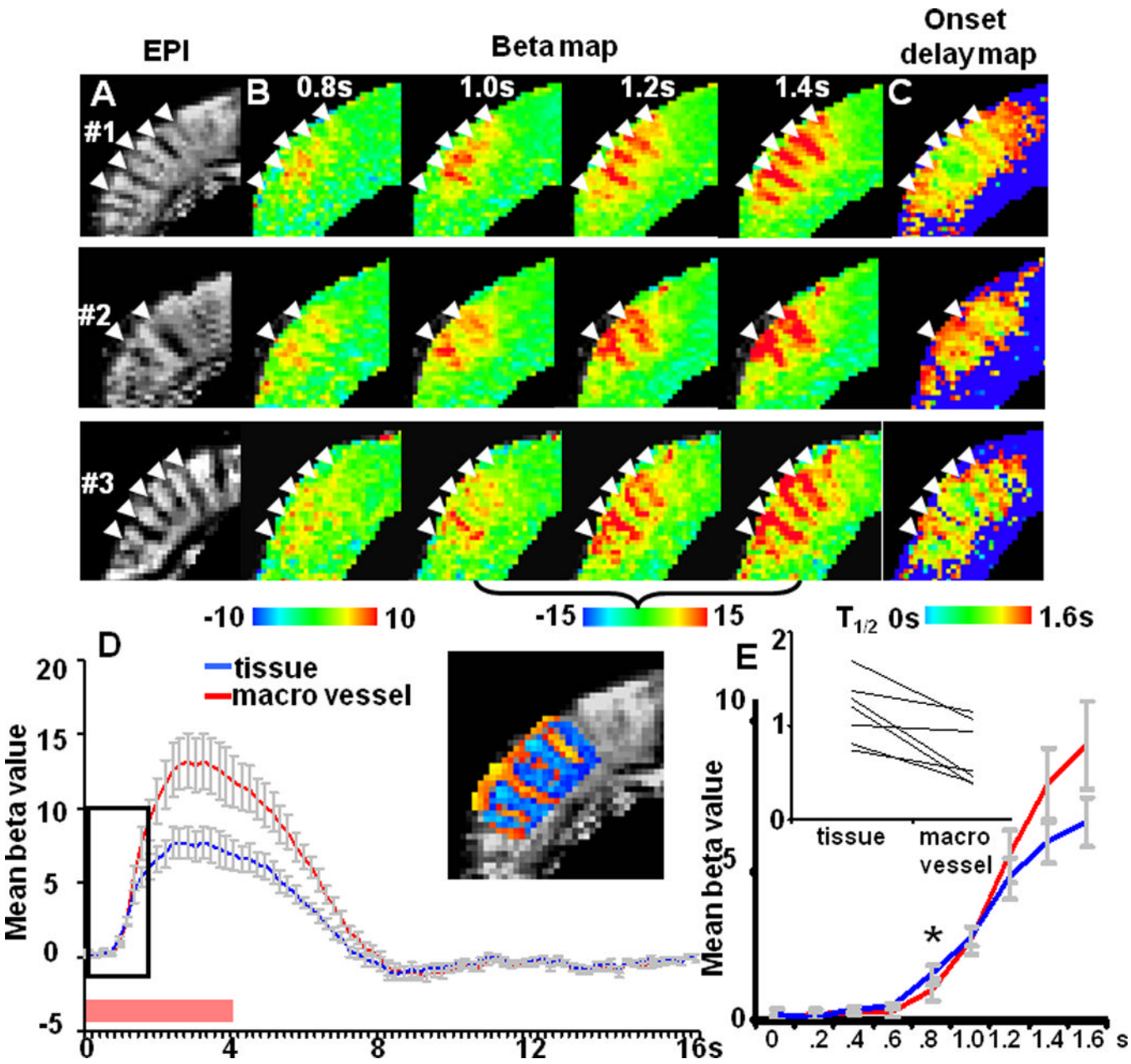

Figure 3.

The spatial pattern of BOLD response from 0.8 to 1.4s from multiple subjects. Intracortical macro vessels are highlighted in EPI images (A, white arrowhead). Beta maps at 0.8, 1.0, 1.2, and 1.4s after stimulation are shown in B. C is the color-coded onset delay map. D is the averaged HRF of macro vessel (red) and tissue (blue) ROIs(inset). E is the enlarged figure of the BOLD response from 0s to 1.6s, showing the higher BOLD signal in tissue ROIs than the macro vessel ROI at 0.8s after stimulation (* mean paired t-test, p=0.009, n=7, error bar is the standard deviation of 7 rats). Mean beta values of tissue and macro vessel ROIs at 0.8s from individual rats are shown in the inset.

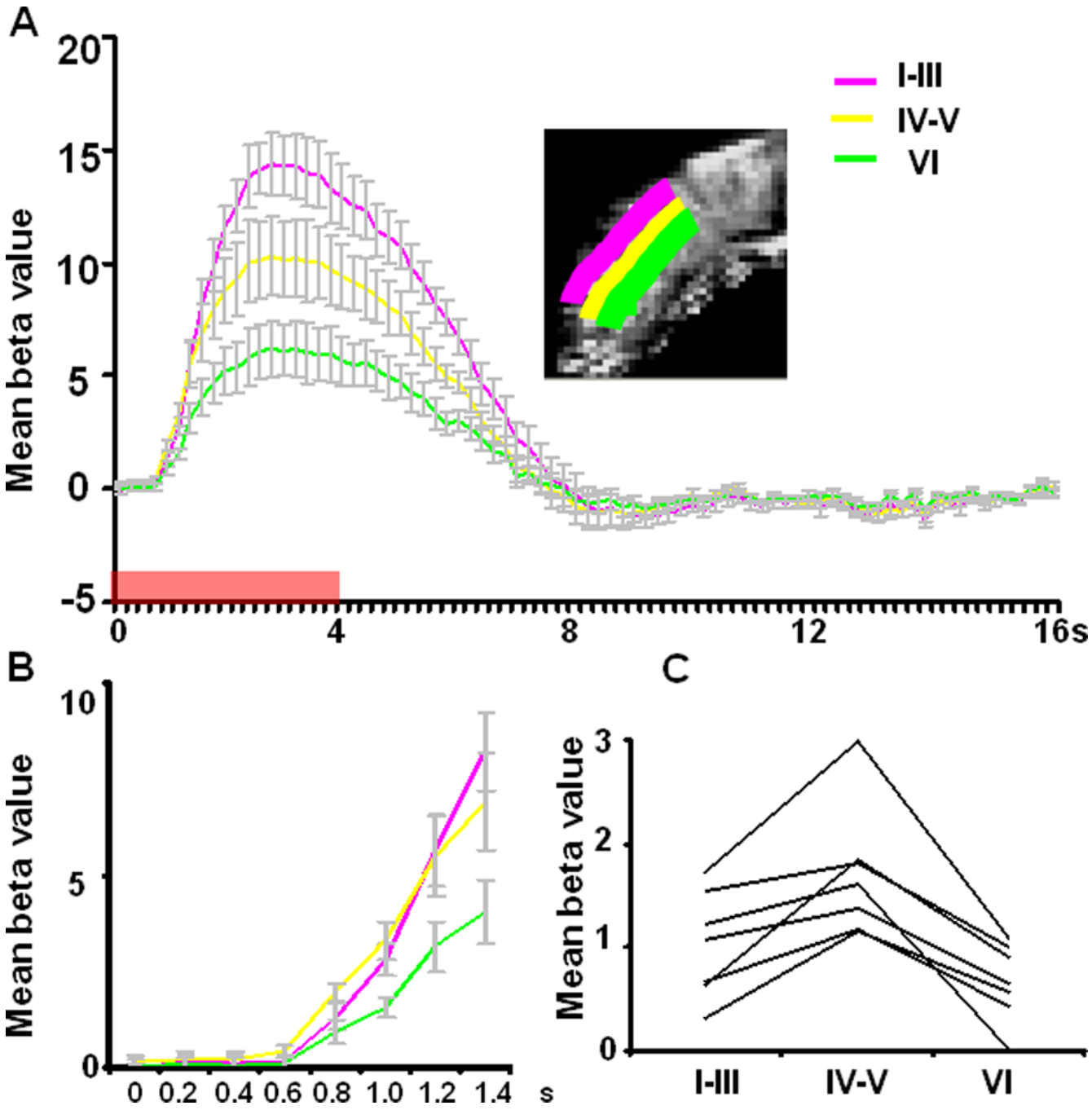

Figure 4.

Layer-specific group ROI analysis of HRF. A is the HRF of ROIs at different cortical layers (I–III in purple, IV–V in yellow, VI in green, inset). The HRF from 0 to 1.4s after stimulation is shown in the enlarged figure (B, error bar is the standard deviation of 7 rats). Mean beta values at 0.8s from individual animals are shown across different layers (C, n=7).

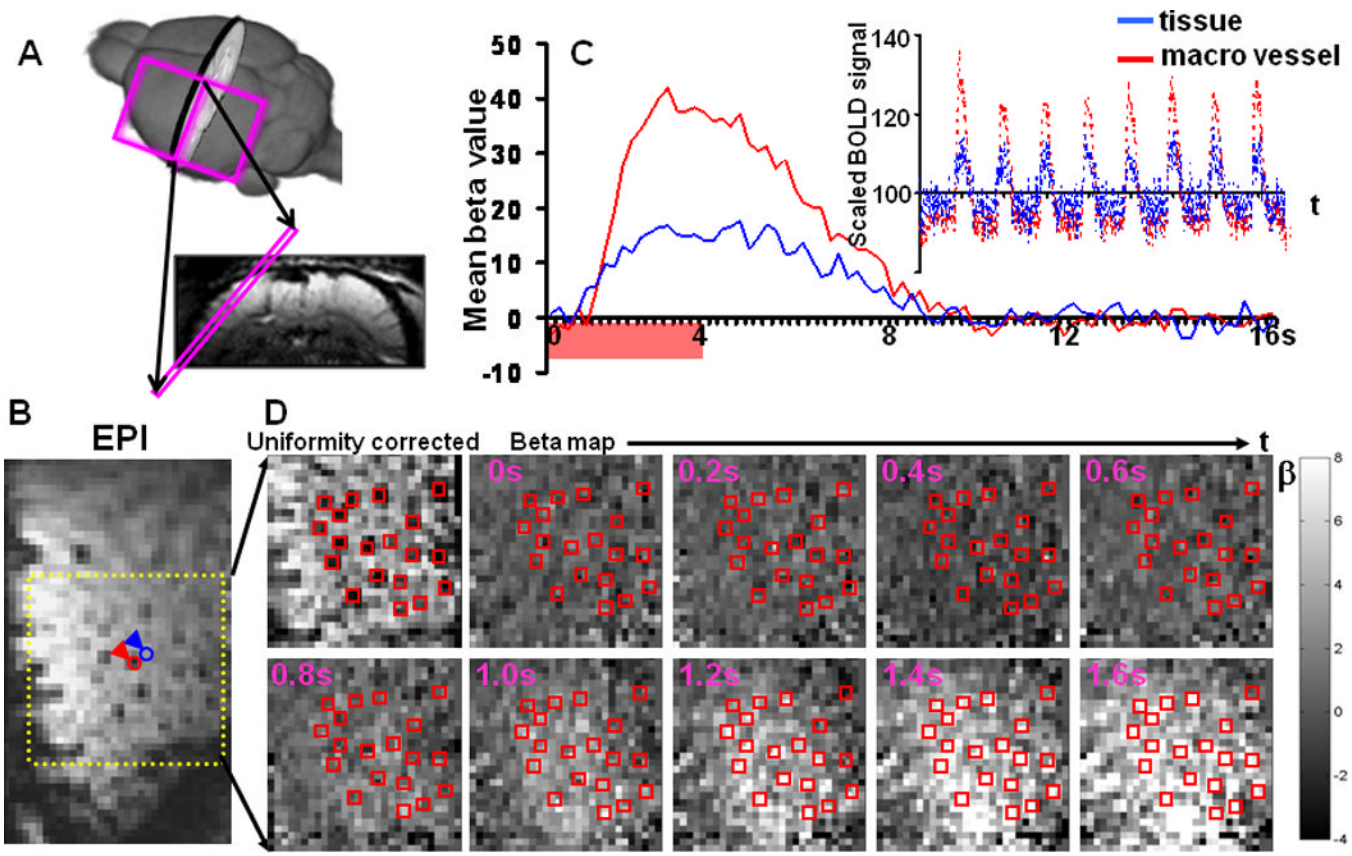

Figure 5.

The spatial pattern of BOLD response in Layer IV–V barrel cortex. The horizontal EPI slice was positioned to cover the layer IV–V of the barrel cortex (A). In the EPI image, the intracortical macro vessel can be visualized as dark dots (B). The HRF of representative single voxels on macro vessel (B, red circle) and adjacent tissue (B, blue circle) is shown in C with the scaled time-courses (inset, dotted line). D shows beta maps at every 200ms from 0s to 1.6s after stimulation with macro vessels highlighted by red squares (D).

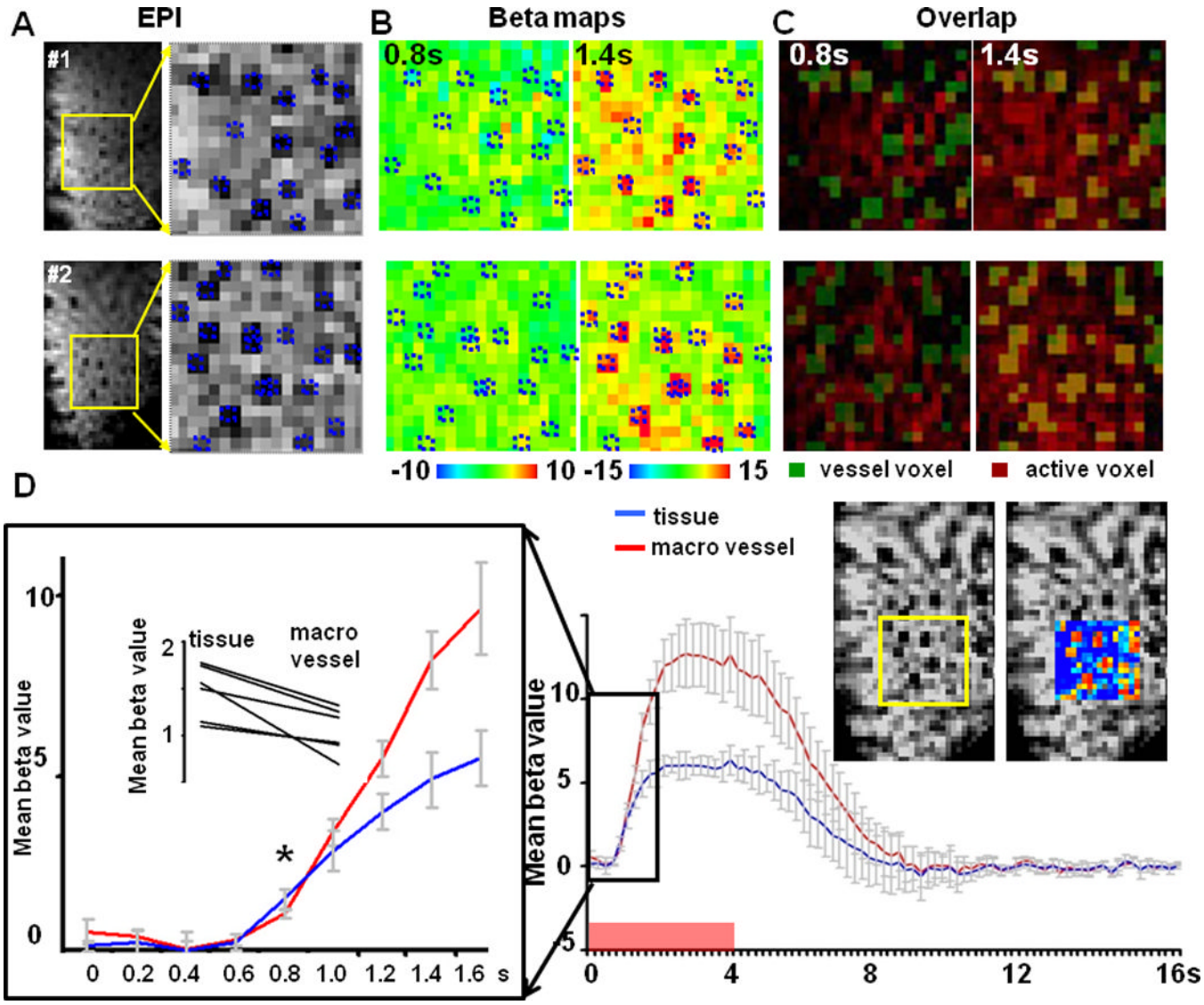

Figure 6.

Group analysis of the early BOLD response in Layer IV–V barrel cortex. A is EPI images across Layer IV–V barrel cortex with uniformity corrected images to show the macro vessels in dotted blue circle. Enlarged beta maps at 0.8s and 1.4s after stimulation are shown to examine the BOLD response in macro vessels (B). C is the overlapped macro vessel (green) with beta maps with active voxels colored in red. The activated macro vessel voxels appeared in yellow (C). D shows the HRF of macro vessel (red) and tissue (blue) ROIs (inset, representative ROIs from rat #2). The enlarged 0–1.6s HFR shows the higher BOLD signal in tissue ROIs than the macro vessel ROI at 0.8s after stimulation (D, * means paired t-test, p=0.0088, n=6, error bar is the standard deviation of 6 rats). Mean beta values of tissue and macro vessel ROIs at 0.8s from individual rats are shown in the inset

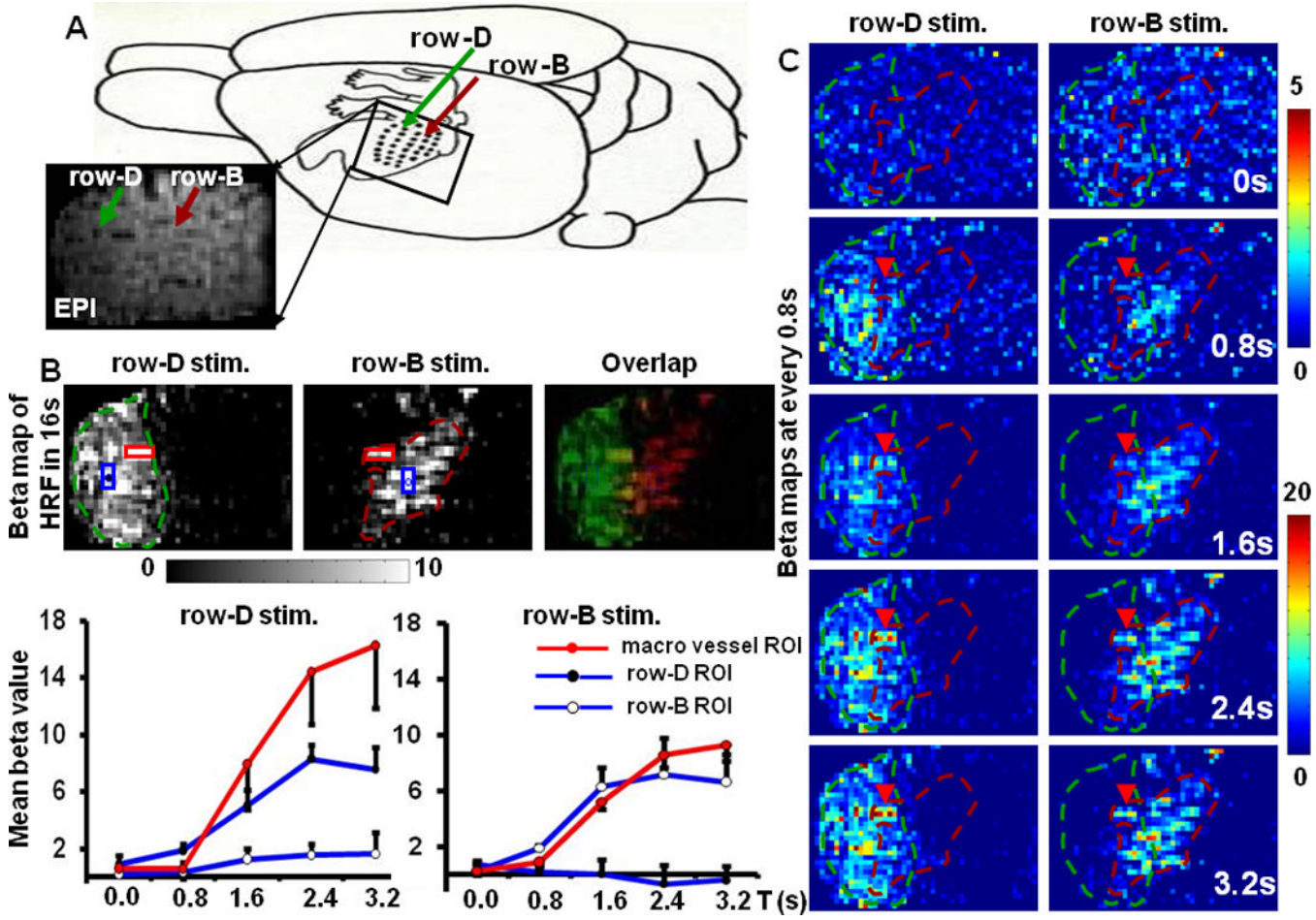

Figure 7.

Mapping the whisker row-B and row-D barrel areas. The orientation of whisker row-B and row-D is shown in the schematic drawing of whisker maps in the barrel cortex and the EPI slice (A). Gray-scale beta maps of row-B and row-D were derived from the linear regression of the total period of the hemodynamic response (B). The two beta maps were overlapped (row-B in red, row-D in green, overlapped active voxels in yellow) and a macro vessel in the overlapped area is highlighted by a red rectangle. Two ROIs were drawn on the centroid of active barrel area for row-B and row-D (B, blue rectangle) to match the macro vessel ROI. The BOLD signal changes of the three ROIs (error bar is the standard deviation of 6 voxels of each ROI) are shown in the lower panel of B. Color-coded beta maps for row-B (C, right) and row-D (C, left) are shown at every 0.8s after stimulation. The macro vessel draining both row-B and row-D barrel area is highlighted by red arrowhead (C).